EBioMedicine 58 (2020) 102925

Contents lists available at ScienceDirect

EBioMedicine

journal homepage: www.elsevier.com/locate/ebiom

Research paper

Vascular occlusion by neutrophil extracellular traps in COVID-19

Moritz Leppkes[a,j,1,*], Jasmin Knopf[b,j,1], Elisabeth Naschberger[c], Aylin Lindemann[a,j], Jeeshan Singh[b,j], Irmgard Herrmann[b], Michael Stürzl[c], Léonie Staats[a,j], Aparna Mahajan[b,j], Christine Schauer[b,j], Anita N. Kremer[d], Simon Völkl[d], Kerstin Amann[e], Katja Evert[f], Christina Falkeis[g], Andreas Wehrfritz[h], Ralf J. Rieker[i], Arndt Hartmann[i], Andreas E. Kremer[a,j], Markus F. Neurath[a,j], Luis E. Muñoz[b,j], Georg Schett[b,j], Martin Herrmann[b,j]

[a] Department of Internal Medicine 1, University Medical Center Erlangen, Friedrich-Alexander-University Erlangen-Nürnberg, Erlangen, Germany
[b] Department of Internal Medicine 3, University Medical Center Erlangen, Friedrich-Alexander-University Erlangen-Nürnberg, Erlangen, Germany
[c] Division of Molecular and Experimental Surgery, Translational Research Center, Department of Surgery, University Medical Center Erlangen, Friedrich-Alexander University Erlangen-Nürnberg, Erlangen, Germany
[d] Department of Internal Medicine 5, Hematology and Oncology, University Medical Center Erlangen, Friedrich-Alexander-University Erlangen-Nürnberg, Erlangen, Germany
[e] Department of Nephropathology, University Medical Center Erlangen, Friedrich-Alexander-University Erlangen-Nürnberg, Erlangen, Germany
[f] Institute of Pathology, University Medical Center Regensburg, Germany
[g] Institut of Pathology, Klinikum Bayreuth, Germany
[h] Department of Anaesthesiology, University Medical Center Erlangen, Friedrich-Alexander-University Erlangen-Nürnberg, Erlangen, Germany
[i] Institute of Pathology, University Medical Center Erlangen, Friedrich-Alexander-University Erlangen-Nürnberg, Erlangen, Germany
[j] Deutsches Zentrum Immuntherapie (DZI), Erlangen, Germany

ARTICLE INFO

Article History:
Received 19 June 2020
Revised 7 July 2020
Accepted 13 July 2020
Available online xxx

Keywords:
SARS-CoV-2
Endothelialitis
Immunothrombosis
Aggregated neutrophil extracellular traps
Coagulopathy

ABSTRACT

Background: Coronavirus induced disease 2019 (COVID-19) can be complicated by severe organ damage leading to dysfunction of the lungs and other organs. The processes that trigger organ damage in COVID-19 are incompletely understood.
Methods: Samples were donated from hospitalized patients. Sera, plasma, and autopsy-derived tissue sections were examined employing flow cytometry, enzyme-linked immunosorbent assays, and immunohistochemistry.
Patient findings: Here, we show that severe COVID-19 is characterized by a highly pronounced formation of neutrophil extracellular traps (NETs) inside the micro-vessels. Intravascular aggregation of NETs leads to rapid occlusion of the affected vessels, disturbed microcirculation, and organ damage. In severe COVID-19, neutrophil granulocytes are strongly activated and adopt a so-called low-density phenotype, prone to spontaneously form NETs. In accordance, markers indicating NET turnover are consistently increased in COVID-19 and linked to disease severity. Histopathology of the lungs and other organs from COVID-19 patients showed congestions of numerous micro-vessels by aggregated NETs associated with endothelial damage.
Interpretation: These data suggest that organ dysfunction in severe COVID-19 is associated with excessive NET formation and vascular damage.
Funding: Deutsche Forschungsgemeinschaft (DFG), EU, Volkswagen-Stiftung

1. Introduction

Coronavirus induced disease 2019 (COVID-19) is a new disease that is caused by Severe Acute Respiratory Syndrome Coronavirus 2 (SARS-CoV-2) that rapidly spreads worldwide[1]. According to the WHO situation report from June 10, 2020; more than 7 million cases globally have been confirmed with more than 400.000 deaths[2]. The reason for the comparatively high mortality in COVID-19 is currently unclear. Initially, severe COVID-19 was considered as an acute respiratory distress syndrome (ARDS) while recently coagulation disorders and thromboembolic events were suspected to contribute to its high mortality[3–6].

Neutrophil activation is an important clinical feature in COVID-19. Patients with severe disease show substantial elevation of circulating neutrophils[7]. Neutrophils are the first responders to invasion of

* Corresponding author at: Department of Internal Medicine 1, University Medical Center Erlangen, Friedrich-Alexander-University Erlangen-Nürnberg, Erlangen, Germany.
E-mail address: moritz.leppkes@uk-erlangen.de (M. Leppkes).
[1] ML and JK equally contributed

https://doi.org/10.1016/j.ebiom.2020.102925

Research in context

Evidence before this study

Recent reports have pointed to a coagulatory disorder and vascular inflammation leading to death in severe Coronavirus induced disease 2019 (COVID-19). SARS-CoV-2 infection promotes endothelialitis that conditions the activation of the innate immune system, especially neutrophils. They may be stimulated to extrude chromatin decorated with granular proteins as neutrophil extracellular traps (NETs).

Added value of this study

In severe COVID-19 neutrophils are highly activated and adopt a low-density phenotype prone to aggregate and form NETs. Strikingly, histopathology of lung autopsies from deceased COVID-19 patients shows congestions of pulmonary micro-vessels by aggregated NETs.

Implications of all the available evidence

This study demonstrates mechanical vessel obstruction by aggregated NETs as a central pathogenic determinant of COVID-19.

pathogens and tissue damage mediating the killing of pathogens by oxidative burst and phagocytosis[8]. Activated neutrophils that fail to extravasate partially degranulate in the circulation[9]. Due to their reduced buoyant densities they are referred to as low-density granulocytes. These cells, which are also found in immune-mediated inflammatory diseases [10] are particularly prone to expulse their chromatin decorated with antimicrobial agents stored in their granules- a process known as neutrophil extracellular trap (NET) formation [11–13].

Previous data suggested that NET formation is involved in pulmonary disease: (i) circulating NETs and their toxic degradation products are increased in patients with transfusion-associated acute lung injury,[14] (ii) neutrophils from pneumonia-associated ARDS are prone to undergo NET formation,[15,16] (iii) extracellular histones are elevated in ARDS,[17] and (iv) NET formation also occurs in COVID-19 patients [18]. Furthermore, excessive NET formation leads to the formation of aggregated NETs [19] that occlude vessels [20] and ducts [21,22] and damage tissues. In this paper, we show that exaggerated NET-formation in COVID-19 contributes to occlusion of pulmonary micro-vessels and thus confers severe organ damage.

2. Materials and methods

2.1. Patients and healthy donors

All patients of this study population (n=71) were recruited from Bavaria, Germany. Serum and cell studies were performed according to the ethical approval using blood samples (serum, citrate plasma, EDTA) from hospitalized patients of the University Hospital Center of Erlangen, Germany. Autopsy material was analyzed from Erlangen, Bayreuth, and Regensburg. Further patient characteristics are described in Table 1.

2.2. Ethical approval

All experiments using human material were performed in accordance with the institutional guidelines and the agreement of the Ethical Committee of the University Medical Center of Erlangen (permit #193_13B and # 174_20B).

2.3. Isolation of leukocytes

Human peripheral blood neutrophils and peripheral blood mononuclear cells (PBMCs) containing the fraction of low-density granulocytes (LDGs) were isolated from EDTA venous blood of healthy donors and patients with COVID-19 by Lymphoflot (Bio-Rad, 824012) density gradient centrifugation. Briefly, whole blood was carefully layered on Lymphoflot solution and centrifuged for 30min at 1400rpm. Plasma was collected and the cells with low buoyant density were harvested. The cells of the high density layer were subjected to hypotonic lysis of RBC. Cells were then counted using the Luna Fl cell counter (Logos Biosystems). Acridine orange/propidium iodide (Logos Biosystems, F23001) staining served to assess cell viability.

2.4. Serum and plasma

Blood was drawn from healthy controls and patients with COVID-19. Disease controls of autoimmune rheumatic diseases (Rheumatoid Arthritis, Systemic Lupus Erythematosus) were measured in parallel (data not shown). Serum and plasma were prepared according to standard laboratory procedures.

2.5. Chemicals and biochemicals

SYTOX™ Green Nucleic Acid Stain - 5 mM Solution in DMSO (ThermoFisher Scientific, S7020), Molecular Probes™ H_2DCFDA (ThermoFisher, Scientific D399), Ionomycin (calcium salt) (Cayman Chemical, 11932), *Klebsiella pneumoniae* lipopolysaccharide (LPS) (Sigma-Aldrich, L4268), Phorbol 12-myristate 13-acetate (PMA) (Cayman Chemical, 10008014), RPMI 1640 Medium without phenol red (ThermoFisher Scientific, 11835063), Lymphoflot Ficoll-Diatrizoate density gradient solution (Bio Rad, 824012), DNase1 (Roche, 11284932001), Heparin-Natrium-25000-ratiopharm® (Ratiopharm).

2.6. Detection of reactive oxygen species

To determine the production of reactive oxygen species (ROS) by neutrophils, 2′,7′-dichlorodihydrofluorescein diacetate (H_2DCFDA, 1•25 μM) was applied. Neutrophils were isolated and stimulated as stated above and ROS production was monitored in a plate reader at 37°C, 5% CO_2 with excitation at 485 nm and emission at 535nm for 4 h.

2.7. Immunophenotyping by flow cytometry

We stained freshly isolated human citrated whole blood with Pacific blue anti-human CD16 (BD Pharmingen, 558122), APC-eFluor780 anti-human CD14 (eBioscience, 47-0149-42) and PE anti-human CD49d (BD Pharmingen, 555503) to identify myeloid subpopulations in both cell fractions. FITC anti-human CD41a (BD Pharmingen, 555475), ECD anti-human CD62L (Immunotech, PN IM2713), PE anti-human CD26 (BD Pharmingen, 555437), FITC anti-human CD66b (Immunotech, 0531), were used for cell surface marker analyses. After RBC lysis and fixation (Q-Prep, Beckman Coulter, Krefeld, Germany) cells were acquired in a Gallios™ flow cytometer (Beckman Coulter) and analyzed using Kaluza 1.5 software (Beckmann Coulter).

2.8. Immunohistochemistry

The pathology department at the University Hospital Erlangen provided biopsies. Lung biopsies from patients with COVID-19, pulmonary emphysema and pulmonary artery embolism and healthy lungs were stained for neutrophil extracellular traps (NETs). General protocol for immunohistochemistry staining (IHC) was followed. Primary unconjugated antibodies for neutrophil elastase (NE) (Abcam,

ab68672) and citrullinated H3 (citH3) (Abcam, ab5103) were diluted in blocking buffer consisting of 10 % FCS, 2 % BSA, 0.1 % Triton X-100 and 0•05 % Tween20 in PBS and incubated for 18 h at 4 °C. A secondary goat anti-rabbit IgG antibody conjugated with fluorophore AF647 (Invitrogen, Alexa Fluoro Plus 647, ab32733) was added for the detection of the primary antibody. The slides were immersed in DAKO fluorescence mounting medium (Agilent technologies, S3023) and analysed on fluorescent microscope BZ-X710 (Keyence Corporation). Permanent CD31 staining was performed after antigen retrieval in TRS pH 9 (Dako Cytomation) using an anti-CD31 antibody (Clone JC70A, DakoCytomation) detected by R.T.U. Vectastain Kit with NovaRed as substrate (both Vector Laboratories) and counterstaining using hematoxylin (Merck KGaA).

2.9. *NET degradation* in vitro

Isolated peripheral blood neutrophils were seeded at a concentration of 50,000 cells per chamber in an 8-chamber glass bottom slide (ThermoFisher Scientfic, 155411) in equilibrated R0 medium (ThermoFisher Scientific, 11835063). NET formation was stimulated with 50 mM HCO_3 for 24 h at 37°C with 5 % CO_2. Subsequently, slides were stained for 15 min at 4°C with SYTOX™ Green (ThermoFisher Scientific, S7020) and washed carefully with PBS. Equilibrated R0 medium supplemented with a final concentration of 1 mM Ca^{2+} and Mg^{2+} was added and pictures were taken on fluorescence microscope BZ-X710 (Keyence Corporation) before and after addition of DNase1 (0•1-1 U/ml) (Roche, 11284932001) and 1-10 U/ml unfractionated heparin (Ratiopharm) at the time points indicated. Z-stacks were employed to increase depth of field. Post-processing of pictures and morphometry was performed employing Photoshop CC 2018 64Bit (Adobe).

2.10. *Quantification of NET degradation products*

2.10.1. *Detection of circulating DNA*

To quantify the amount of circulating cell-free DNA in the plasma of patients with COVID-19 compared to healthy controls, the Quant-iT™ PicoGreen™ dsDNA Assay-Kit (ThermoScientific, P11496) was employed according to manufacturer's instructions. Briefly, samples were diluted 1:20 in TE buffer and Quant-iT™ PicoGreen™ dsDNA reagent was added in a 1:1 ratio. After incubation for 5 min at RT in the dark, the fluorescence was read in an Infinite® 200 PRO plate reader (Tecan; ex. 485 nm, em. 535 nm). The concentration of the circulating cell-free DNA was calculated with the standard provided by the kit using Excel (Microsoft).

2.10.2. *Detection of citrullinated Histone H3 in serum*

The presence of citrullinated Histone H3 as surrogate marker for neutrophil extracellular traps (NETs) was estimated with a citrullinated Histone H3 ELISA (Cayman Chemical). The ELISA was performed according to the manufacturer's instructions using serum samples from healthy controls, patients with COVID-19 and patients with autoimmune rheumatic diseases (Rheumatoid Arthritis, Systemic Lupus Erythematosus) (data not shown).

2.10.3. *Detection of total protein citrullination in serum*

The overall protein citrullination in serum was estimated using the anti-citrulline (modified) Detection Kit (Merck KGaA 17-347B). To this end, sera were coated overnight at +4 C in coating buffer (0.1 M Na_2CO_3, 0.1 M $NaHCO_3$, pH 9.6) in a 96-well maxisorp immuno-plate (ThermoFisher Scientific, 442404). The next day, a mixture of reagent A and B from the kit was added to the wells overnight at +37°C. Then, the plate was blocked with 5% BSA in TBS-T before the anti-citrulline modified antibody from the kit was added, followed by the detection antibody goat-anti-human HRP conjugated from the same kit. The reaction was developed with TMB substrate set (BioLegend,421101) and OD values were read at 450 nm with a reference at 620 nm in a SUNRISE microplate reader (Tecan).

2.10.4. *Detection of NE-DNA and MPO-DNA complexes in plasma*

The presence of circulating NE-DNA and myeloperoxidase (MPO)-DNA complexes in citrate plasma of patients with COVID-19 and healthy controls was detected using an ELISA. To this end, anti-NE or anti-MPO antibody (Abcam, ab21595 and ab9535) were coated to 96-well maxisorp immuno-plates overnight at +4°C in coating buffer (0.1 M Na_2CO_3, 0.1 M $NaHCO_3$, pH 9.6). The next day, plates were blocked with 3% BSA in PBS and 25μl citrate plasma was incubated overnight at +37°C. NE-DNA or MPO-DNA complexes were detected using the peroxidase-conjugated anti-DNA POD from the Cell Death Detection ELISA (Roche, 11544675001). The reaction was developed using TMB substrate set (BioLegend) and the ODs were read at 450 nm with a reference at 620 nm in a SUNRISE microplate reader (Tecan).

2.10.5. *Detection of Neutrophil Elastase (NE) Activity*

The activity of NE in plasma was assessed using the fluorogenic substrate MeOSuc-AAPV-AMC (Santa Cruz Biotechnology, sc-201163) to a final concentration of 100 μM. The specificity was further evaluated using the NE specific inhibitor Sivelestat (Sigma-Aldrich,S7198) to a final concentration of 250 μM for 24 h at 37 C. Fluorescent readings at 37 C were collected on a TECAN Infinite 200 Pro using the filter set ex. 360 nm, em. 465 nm for 24 h in a 20 min interval.

2.10.6. *Quantification of cytokines*

Cytokines in serum were quantified using a custom-made LEGENDplex™ bead-based immunoassay (BioLegend) according to manufacturer's protocol. Briefly, serum was diluted in assay buffer and incubated for two hours at RT shaking with the beads and the detection antibody. Streptavidin-Phycoerythrin was added subsequently. After washing cytokines were quantified using a Gallios Flow Cytometer (Beckman Coulter) followed by analyses employing Kaluza 1.5 analysis software (Beckman Coulter) and Excel (Microsoft). MCP-3 was quantified in the citrate plasma of patient's with COVID-19 and healthy controls using the human CCL7/MCP-3 DuoSet ELISA (R&D systems, DY282) according to manufacturer's instructions.

2.10.7. *Statistics*

The present is an observational case-control study. For comparisons between two independent groups, Mann−Whitney U-tests for numerical variables and exact χ^2-tests for nominal characteristics were employed. For comparisons among three groups the non-parametric Kruskal-Wallis-test with Dunn's multiple comparisons post-test correction was applied. Associations between clinical and laboratory variables were measured by Spearman rho correlation coefficients. A sample size calculation was performed using the software G*power. For the testing differences among three independent means, a total sample size of 25 individuals ($n \geq 6$ each group) would be needed to detect an effect size f of 1.0 with 80% power and an alpha error at $\alpha = 0.05$ by using the ANOVA test with fixed effects. For two independent means a total sample size of 28 individuals would be needed to detect an effect size f of 1.0 with 80% power and an alpha error at $\alpha = 0.05$ by using the t-test. The actual power increases with the sample size for each parameter accordingly. Due to the unpredictable availability of samples, various samples sizes are depicted. Groups with $n < 6$ or $n < 14$ were excluded from the Kruskal-Wallis and Mann-Whitney U-Tests, respectively. Statistical calculations were performed using IBM SPSS (version 24) and GraphPad Prism 8.3.0 softwares. A P value ≤ 0.05 was considered statistically significant and indicated in the figures.

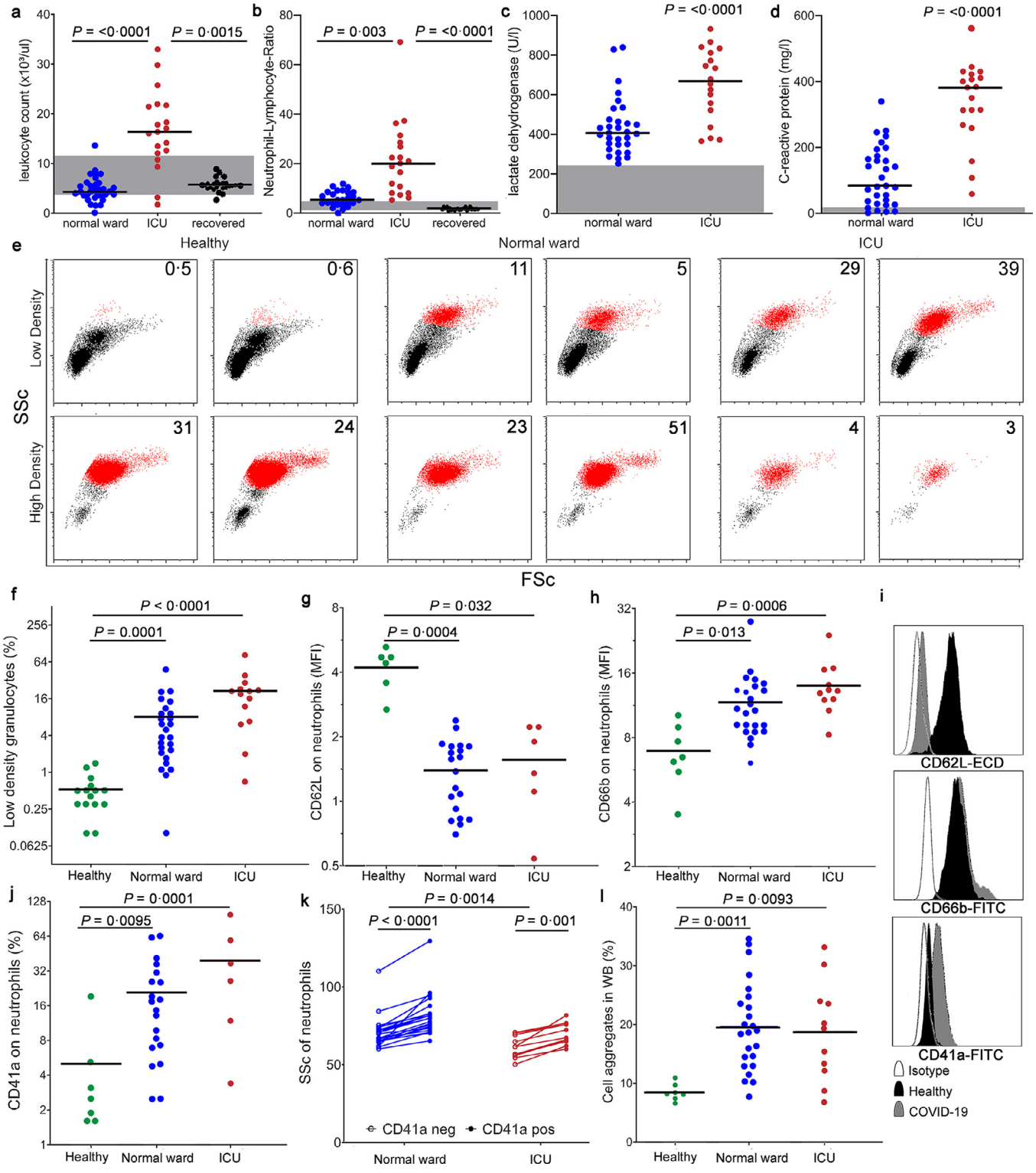

Fig. 1. During acute phase responses in patients with COVID-19 circulating neutrophils display an activated, post-secretory phenotype prone to cellular aggregation.

(a) Leukocyte count (Kruskal-Wallis $P<0.0001$) and (b) the neutrophil-lymphocyte ratio are elevated in severe COVID-19 (Kruskal-Wallis $P<0.0001$). Elevations of (c) lactate dehydrogenase (LDH) and (d) C-reactive protein (CRP) serum levels discriminate normal ward and ICU patients with COVID-19. The respective reference range is highlighted in grey. (e,f) Increased amounts of neutrophils are recovered from the low buoyant-density fraction after centrifugation. Numbers indicate percentage of CD16+ neutrophils of leukocytes of both densities (Kruskal-Wallis $P<0.0001$). (g,i upper panel) Downregulation of CD62L (Kruskal-Wallis $P=0.0007$) and (h,i middle panel) upregulation of CD66b in circulating neutrophils (Kruskal-Wallis $P=0.001$). (i lower panel, j, k) The activated phenotype of neutrophils is associated with an enhanced interaction with thrombocytes (CD41a) (Kruskal-Wallis $P=0.0002$) and (l) other leucocytes in whole blood precipitating cellular aggregation in patients in whole blood (WB) (Kruskal-Wallis $P=0.0013$) (green: healthy donors; blue: patients treated in normal wards; red: patients treated in intensive care units (ICU); black: patients recovered from COVID-19. Single dots represent individual patient samples. Kruskal-Wallis test was used for multiple group comparisons and the respective P value is depicted in the figure legend, P in the figure is deduced from post-hoc pair-wise comparison using Dunn's test) (For interpretation of the references to color in this figure legend, the reader is referred to the web version of this article).

3. Results

3.1. Increase of activated low-density and platelet-decorated granulocytes in COVID-19

We first analyzed circulating neutrophils in mild (normal ward) and severe (intensive care unit, ICU) COVID-19 patients. We recognized significant elevation of leukocytes (Fig. 1a) and increased neutrophil-lymphocyte ratio (Fig. 1b) in severe compared to mild disease and compared to those patients recovered from COVID-19. In accordance, chemokines MCP-3 and IL-8 indicative of myeloid and neutrophil chemo-attraction were significantly increased in the circulation in both mild and severe COVID-19 patients (Fig. S1a,b). Other cytokines and chemokines were consistently upregulated in COVID-19 patients (Fig. S1c-g): IL-6, IL-8, IL-18, and MCP3 discriminated severe from milder forms of the disease. Significantly increased levels of lactate dehydrogenase (LDH) indicating cellular demise and C-reactive protein (CRP) indicating an acute phase response were also found in severe COVID-19, as previously reported (Fig. 1c,d).

Closer analysis of the leukocytes in COVID-19 patients showed significant increases in the numbers of neutrophils with low buoyant density (Fig. 1e,f), activation pattern (low L-selectin, CD62L; Fig. 1g,i), and partial degranulation (increased CEACAM-8, CD66b; Fig. 1h,i and reduced side scatter (SSc); Fig. 1k) resembling low-density granulocytes. Furthermore, neutrophils were decorated with thrombocytes in COVID-19, especially in severe disease (Fig. 1i-k) and formed multicellular aggregates (Fig. 1l). When isolating neutrophils from COVID-19 patients the cells exhibited an exhausted phenotype with reduced spontaneous oxidative burst in response to lipopolysaccharide (LPS) (Fig.S2).

3.2. Circulating fibrin- and NET-degradation products characterize severe COVID-19

When we analyzed plasma of COVID-19 patients, levels of D-dimers and cell free DNA were elevated and particularly high in patients with severe disease indicating enhanced coagulation and NET turnover, respectively (Fig. 2a-d). In accordance, DNA-myeloperoxidase (MPO) and DNA-neutrophil elastase (NE) complexes were significantly higher in COVID-19 patients compared to healthy donors (Fig. 2e,f). Furthermore, citrullination of histone H3 (citH3) (Fig. 2g) and of serum proteins (Fig. 2h) was increased in COVID-19 patients and the former also discriminated mild from severe disease. Both citH3 and cell-free DNA positively correlated with leukocyte and granulocyte counts, respectively (Fig. S3a-d, Table 2). Cell-free DNA further correlated positively with CRP and LDH (Fig. S3e,f). Notably, NE activity in the blood was more than 30- and 60-fold increased in mild and severe COVID-19 patients, respectively, compared to healthy subjects (Fig. S4a). Surprisingly, patient sera strongly inhibited extrinsic NE activity, indicating that the circulating enzyme was partially resistant to its endogenous inhibitor α1-antitrypsin (Fig. S4b).

3.3. Vascular occlusion by neutrophil extracellular traps in COVID-19

Activated neutrophils tend to aggregate and are prone to form NETs at high cellular densities.[19] NETs themselves aggregate and reportedly occlude tubular structures.[20,21] We, therefore, analysed autopsy-derived lung tissues from eight patients with COVID-19 for the presence of ductal occlusion. Strikingly, we found that the main structure occluded by aggregated NETs are pulmonary vessels (Fig. 3a-d, Fig. S5-7, Table 3). Cell-rich intra-vascular clots contained

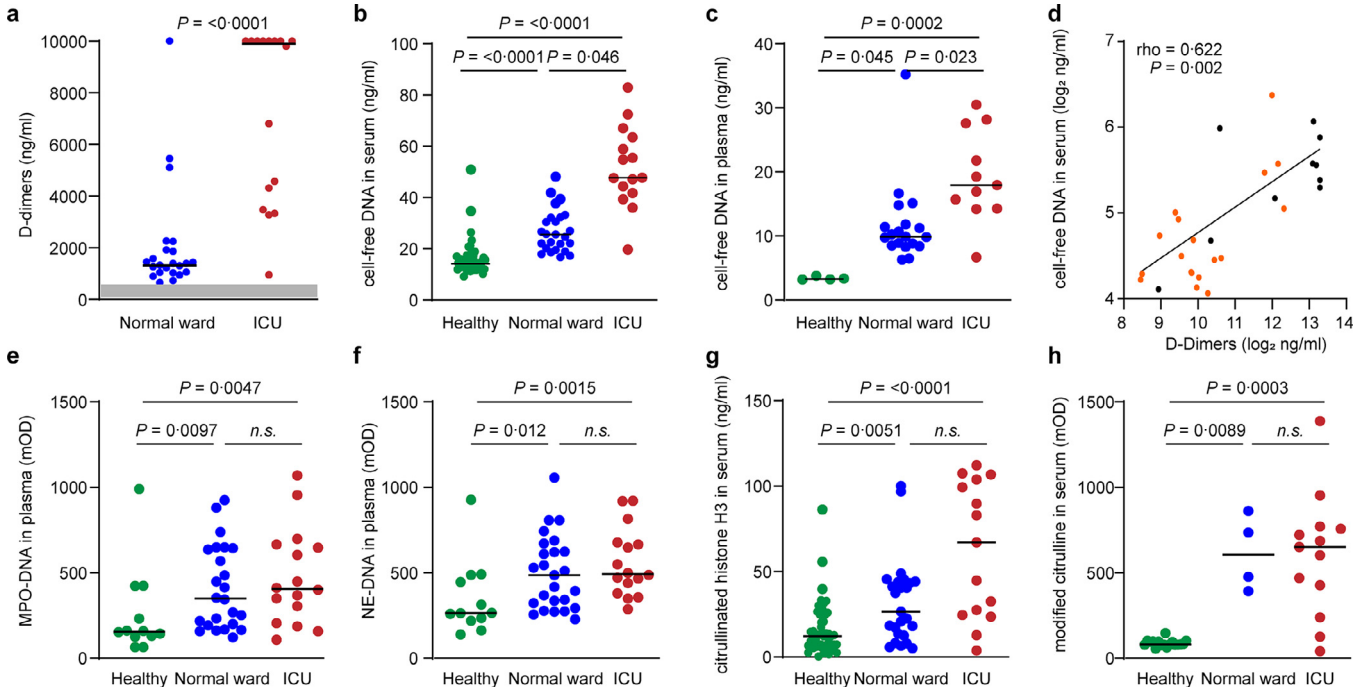

Fig. 2. Fibrin- and NET degradation products are elevated in the circulation during severe COVID-19

(a) The cross-linked fibrin degradation products (D-dimers) are elevated in hospitalized patients with COVID-19 and are strongly increased in patients requiring ICU care. The reference range is highlighted in grey. (b) Cell-free DNA was elevated in both serum (Kruskal-Wallis $P<0.0001$) and (c) plasma (Kruskal-Wallis $P=0.0002$) and (d) correlated with the D-dimer level (orange/black represents survivors/non-survivors). NET degradation products, namely (e) myeloperoxidase-DNA complexes (MPO-DNA) in citrated plasma (Kruskal-Wallis P=0.0033), (f) neutrophil elastase-DNA complexes (NE-DNA) in citrated plasma (Kruskal-Wallis P=0.0017) and (g) citrullinated histone H3 in serum were increased in the circulation of patients as compared to healthy controls (Kruskal-Wallis P=0.0001). (h) Modified protein-bound citrulline was significantly elevated in serum proteins of hospitalized patients (Kruskal-Wallis P<0.0001). (green: healthy donors; blue: patients treated in normal wards; red: patients treated in intensive care units (ICU). Single dots represent individual patient samples; Kruskal-Wallis test was used for multiple group comparisons and the respective P value is depicted in the figure legend, P in the figure is deduced from post-hoc pair-wise comparison using Dunn's test) (For interpretation of the references to color in this figure legend, the reader is referred to the web version of this article).

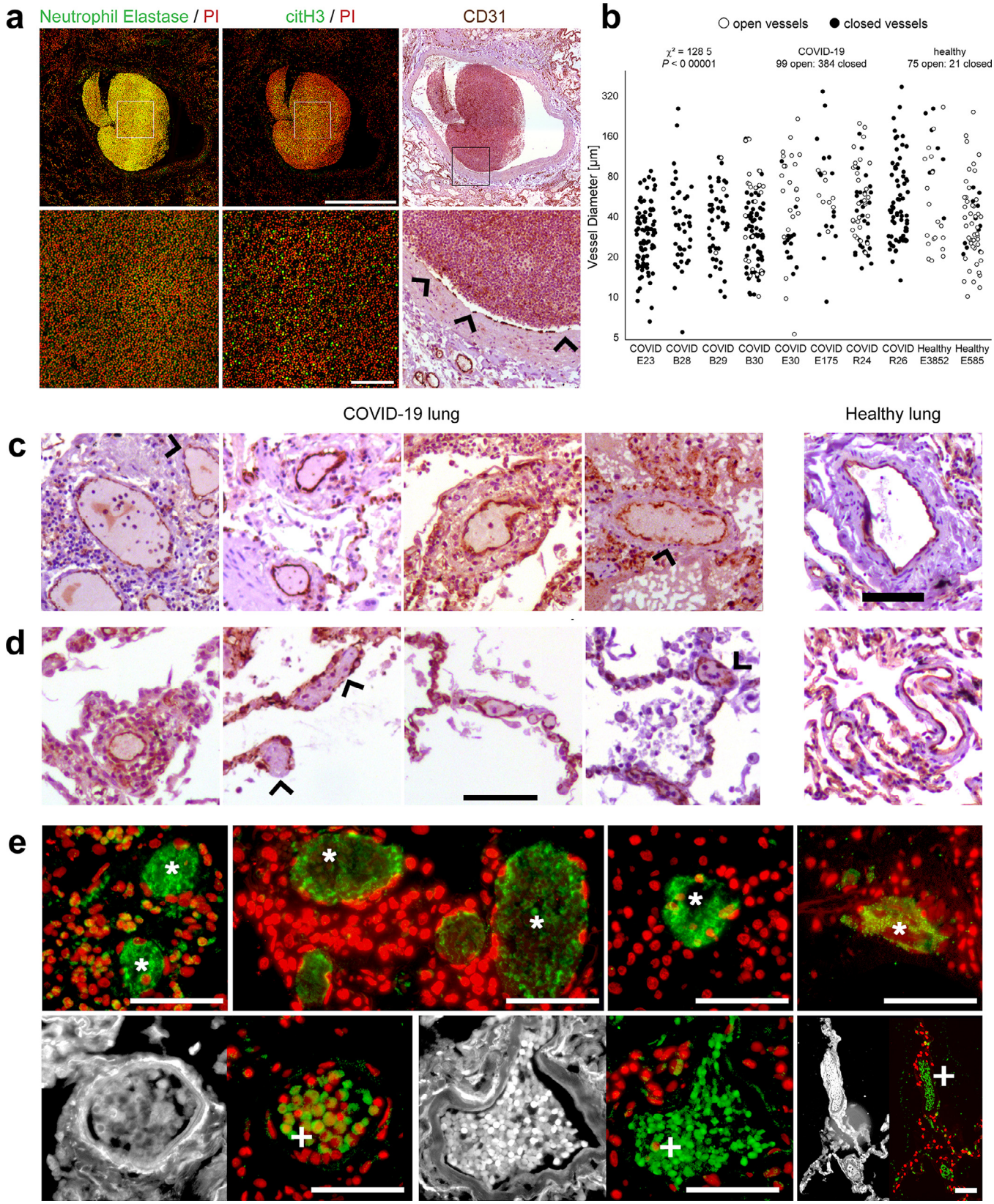

Fig. 3. Aggregated neutrophil extracellular traps occlude pulmonary vessels.

Immunohistochemistry was performed on lung tissue sections derived from autopsies of COVID-19 patients (n=8). (a) A representative picture of an occluded pulmonary blood vessel (CD31) is shown. The occlusive material is immunopositive for DNA (propidium iodide (PI) (red)), neutrophil elastase and citrullinated histone H3 (citH3) (green) typical of neutrophil extracellular traps and characterized by a high cellularity (scale bars designate 1 mm (upper panel) and 100 μm (lower panel), arrowheads indicate areas of endothelial damage). (b) Using CD31 immunohistochemistry open and occluded vessels were quantified in each lung tissue section of deceased COVID-19 patients and 2 non-COVID-19 control samples (single dots represent individual blood vessels, empty circles represent open vessels, filled circles represent occluded vessels). (c) Small and middle-sized vessels from COVID-19 sections were frequently clotted as compared to vessels in healthy control sections (Scale bars designate 100 μm, arrowheads indicate areas of endothelial damage). (d) Capillaries in dilated alveolar septa were frequently clogged with pauci-cellular material (Scale bars designate 200 μm, arrowheads indicate areas of endothelial damage). (e) Lung

vast amounts of aggregated neutrophils that express neutrophil elastase (Fig. 3a, left panel) and citrullinated histone H3 (Fig. 3a, middle panel). The adjacent vessel wall was partially denuded of CD31+ endothelial cells indicating endothelial cell damage next to this neutrophil clot. Smaller vessels often showed preserved endothelia (Fig. 3c). Especially the microvasculature along the alveolar septa was strongly affected (Fig. 3d). It was clogged by either DNA co-localizing with neutrophil elastase (appearing as pauci-cellular plugs) (Fig. 3e, Fig. S6a and Fig. S7a) or aggregates of nucleated cells containing citrullinated nuclei (appearing as cell-rich occlusions) (Fig. S6b and Fig. S7b). This suggests a dynamic morphology of aggregated NETs. The number of CD31 positive vessels occluded by aggregated NETs was highly increased in COVID-19 patients (Fig. 3b). In addition, analyses of kidney and liver tissues from COVID-19 patients also showed the presence of aggregated NETs with expression of NE and citH3 in the damaged glomeruli and hepatic periportal fields (Fig. S8). NET formation and aggregation may thus drive multi-organ damage in COVID-19.

3.4. Heparin promotes the degradation of neutrophil extracellular traps by DNase1

Under homeostatic conditions, the vasculature is protected from NET formation by circulating DNase1 and DNase1L3, rapidly degrading circulating NETs. However, under inflammatory conditions homeostatic NET degradation mechanisms may be locally overwhelmed precipitating vascular occlusion (Fig. 3). Cleavage of neutrophil chromatin will result in soluble NET degradation products with preserved (histone-mediated) toxicity. Therapeutic strategies need to prevent NET formation, enhance NET degradation and neutralize toxic degradation products. While DNase1 alone only slowly cleaved NETs, the addition of unfractionated heparin strongly accelerated this clearance process *in vitro* (Fig. S9). This underlines the dual functions of heparin, namely inhibition of plasmatic coagulation and dissolution of NET-driven vascular occlusion in the treatment of severe COVID-19.

4. Discussion

A substantial part of the immune pathogenesis of COVID-19 is driven by neutrophil activation. In this study, we show that COVID-19, in particular severe disease, is associated with excessive, i.e. intravascular neutrophil aggregation and NET formation. While increased circulating neutrophils have already been described as feature of more severe courses of COVID-19, data from this study show that the disease leads to significant increase of “low density granulocytes” a specific form of neutrophils that also occurs in autoimmune disease [10] and have a high propensity to spontaneously form NETs. IL-8, which orchestrates recruitment of neutrophils to inflammatory sites was elevated in COVID-19 patients and several indicators of enhanced NET turnover prevailed. Indeed, we observed robust increases of circulating DNA, citrullinated histone H3, MPO- and NE-DNA complexes, and NE activity. Robust correlations with disease severity were especially detected in assays, which are less vulnerable to interference by NE activity [23]. NE activity in sera was enhanced despite the presence of functional endogenous inhibitors of NE, possibly due to DNA binding [24].

While limited amount of NET formation at inflammatory sites in the context of increased neutrophil migration is part of the bodies defense against pathogens, NET formation in COVID-19 is clearly dysregulated, as it occurs at multiple intra-vascular sites and leads to rapid occlusion of pulmonary micro-vessels. Neutrophil aggregates and neutrophil-platelet aggregates in the blood of COVID-19 patients illustrate this process. Even vascular occlusion by neutrophil aggregates and NETs may be beneficial on a small scale to contain an inflammatory focus, but the occurrence of neutrophil-mediated occlusions in a severe COVID-19 infection on a larger scale precipitates respiratory insufficiency. Deleterious intravascular NET formation is usually prevented by the intrinsically high DNase activity in the blood, which seems to be overstretched in COVID-19. NETs in the vascular system activate vascular endothelial cells,[25] favor platelet aggregation[26] and induce plasmatic coagulation via the activation of factor XII [27,28]. Furthermore, NET-mediated citrullination has shown to maintain venous thrombi [29,30] and also interferes with the anti-coagulatory surface properties of the endothelium exemplified by thrombomodulin degradation by neutrophil elastase [31]. In accordance we found numerous pulmonary micro-vessels, which were occluded either by neutrophil aggregates or by neutrophil-derived DNA sludge.

This remarkable neutrophil aggregation and NET formation in micro-vessels in COVID-19 is most likely based on endothelial damage resulting from viral infection. Next to alveolar cells, also endothelial cells provide a rich source of expression of ACE2, the receptor for SARS-CoV-2, while neutrophils themselves do not express ACE2 [32–34]. Endothelial cell infection and death reportedly occurs in COVID-19,[35,36] which most likely associates with the findings of “thromboembolic” events in the lungs of COVID-19 patients [37,38]. Endothelial cell damage, as exemplified by localized disappearance of pulmonary CD31+ endothelial cells, may constitute an important trigger for neutrophil attraction and NET formation. This concept is supported by evidence of co-localization of endothelial damage and neutrophil aggregates.

Reminiscent of our current findings, neutrophilic capillaritis has been described in pulmonary manifestations of immune-mediated inflammatory diseases, antibody-mediated transplant rejections, and rarely in infections [39–41]. Neutrophil-mediated vascular occlusion is thus not specific for severe COVID-19, but occurred in an unexpectedly pronounced intensity in select patients.

Preventing excessive NET formation and limiting heterotypic and homotypic neutrophil aggregation may provide an approach to inhibit vascular occlusion and the development of severe COVID-19 [42]. This could be realized by dexamethasone-inhibited cell aggregation [43] and inhibitors of NET formation, like those targeting PAD4 enzymes [44]. Such anti-inflammatory strategies may come at the risk of increased bloodstream infections which strongly varies among agents currently in use [45].

On the other hand, our data also shows that heparin effectively dismantles NET chromatin and thus strengthens the degradation ability of endogenous circulating DNase1. Indeed, it has been shown that sequestration of histones by heparin further inhibits their function as danger signal and precipitators of inflammation [46]. These findings are also in accordance with previous data showing that heparin mitigates NET formation [47] and the inflammatory consequences of NETs[48]. The right dose is critical as histones interfere with the anti-coagulatory capacity of heparin [49]. Standard prophylactic dose may not be sufficient in severe COVID-19 due to increased circulating NET-derived histones[38]. In summary, this study shows that excessive NET formation drives immunopathology in severe COVID-

tissue sections of deceased COVID-19 patients were stained for expression of neutrophil elastase. The autofluorescence signal (488/525 nm) is displayed side-by-side in greyscale to identify vascular structures. Intermediate-sized pulmonary vessels from COVID-19 patients were frequently clotted by NETs (Scale bar designates 100 μm, asterisks and crosses indicate vessels clogged by pauci-cellular NETs and neutrophil-rich aggregates, respectively) (For interpretation of the references to color in this figure legend, the reader is referred to the web version of this article.).

19-associated disseminated pulmonary intravascular coagulopathy (Table 4)[50].

Author contributions

I.H., M.H., J.K., A.L., M.L., A.M., L.E.M., E.N., C.S., J.S., L.S., and S.V. performed experiments. K.A., K.E., C.F., A.H., and R.R. conducted autopsies and performed pathological analyses. A.E.K., A.N.K., and A. W. coordinated patient sample acquisition and ethical approval of the study. M.H., J.K., M.L., L.E.M., M.F.N, G.S, and M.S. conceived the study, coordinated experiments, and conducted data analyses. All authors provided scientific input, wrote, read, and approved the manuscript.

Declaration of Competing Interest

Martin Herrmann served as adviser to Neutrolis, Cambridge, MA. The remaining authors declare no financial competing interests related to the study.

Acknowledgments

The authors acknowledge support by Deutsche Forschungsgemeinschaft (DFG) and Friedrich-Alexander Universität Erlangen-Nürnberg (FAU). This work was partially supported by the German Research Foundation (DFG) (SCHA 2040/1-1; SCHE1583714-1; TRR241: B04; CRC1181: C03, A01, Z02; SFB 1350: C2; FOR 2886 projects A03, B03, FOR 2438 (to EN/MST), by the EU (H2020-MSCE-RISE-2015 project Nr. 690836 PANG; ERC-Synergy grant 4D Nanoscope), by the Volkswagen-Stiftung (Grant 97744), and by local funds of the Interdisciplinary Center for Clinical Research (IZKF) and ELAN of the FAU (C.S.). We thank Christian Flierl for excellent technical assistance. The present work was performed by L.S. as part of the requirements for obtaining the degree “Dr. med.” conferred by the Friedrich-Alexander-University Erlangen-Nürnberg, Germany (FAU). The funders had no role in study design, data collection, data analysis, interpretation, or writing of the report

Supplementary materials

Supplementary material associated with this article can be found, in the online version, at doi:10.1016/j.ebiom.2020.102925.

References

[1] Zhu N, Zhang D, Wang W, et al. A Novel Coronavirus from Patients with Pneumonia in China, 2019. N Engl J Med 2020;382(8):727–33.
[2] WHO. Coronavirus disease 2019 (COVID-19) Situation Report –142. 10.06.2020 2020. https://www.who.int/docs/default-source/coronaviruse/situation-reports/20200610-covid-19-sitrep-142.pdf?sfvrsn=180898cd_6. Accessed 11.06.2020 2020).
[3] Huang C, Wang Y, Li X, et al. Clinical features of patients infected with 2019 novel coronavirus in Wuhan, China. Lancet 2020;395(10223):497–506.
[4] Liu Y, Yan LM, Wan L, et al. Viral dynamics in mild and severe cases of COVID-19. Lancet Infect Dis 2020.
[5] Tang N, Li D, Wang X, Sun Z. Abnormal coagulation parameters are associated with poor prognosis in patients with novel coronavirus pneumonia. J Thromb Haemost 2020;18(4):844–7.
[6] Chen N, Zhou M, Dong X, et al. Epidemiological and clinical characteristics of 99 cases of 2019 novel coronavirus pneumonia in Wuhan, China: a descriptive study. Lancet 2020;395(10223):507–13.
[7] Lagunas-Rangel FA. Neutrophil-to-lymphocyte ratio and lymphocyte-to-C-reactive protein ratio in patients with severe coronavirus disease 2019 (COVID-19): A meta-analysis. J Med Virol 2020.
[8] Jenne CN, Liao S, Singh B. Neutrophils: multitasking first responders of immunity and tissue homeostasis. Cell Tissue Res 2018;371(3):395–7.
[9] Adrover JM, Aroca-Crevillen A, Crainiciuc G, et al. Programmed 'disarming' of the neutrophil proteome reduces the magnitude of inflammation. Nat Immunol 2020;21(2):135–44.
[10] Carmona-Rivera C, Zhao W, Yalavarthi S, Kaplan MJ. Neutrophil extracellular traps induce endothelial dysfunction in systemic lupus erythematosus through the activation of matrix metalloproteinase-2. Ann Rheum Dis 2015;74(7):1417–24.
[11] Brinkmann V, Reichard U, Goosmann C, et al. Neutrophil extracellular traps kill bacteria. Science 2004;303(5663):1532–5.
[12] Schonrich G, Raftery MJ. Neutrophil Extracellular Traps Go Viral. Front Immunol 2016;7:366.
[13] Boeltz S, Amini P, Anders HJ, et al. To NET or not to NET:current opinions and state of the science regarding the formation of neutrophil extracellular traps. Cell Death Differ 2019;26(3):395–408.
[14] Caudrillier A, Kessenbrock K, Gilliss BM, et al. Platelets induce neutrophil extracellular traps in transfusion-related acute lung injury. J Clin Invest 2012;122(7):2661–71.
[15] Bendib I, de Chaisemartin L, Granger V, et al. Neutrophil Extracellular Traps Are Elevated in Patients with Pneumonia-related Acute Respiratory Distress Syndrome. Anesthesiology 2019;130(4):581–91.
[16] McDonald B, Urrutia R, Yipp BG, Jenne CN, Kubes P. Intravascular neutrophil extracellular traps capture bacteria from the bloodstream during sepsis. Cell Host Microbe 2012;12(3):324–33.
[17] Lv X, Wen T, Song J, et al. Extracellular histones are clinically relevant mediators in the pathogenesis of acute respiratory distress syndrome. Respir Res 2017;18(1):165.
[18] Zuo Y, Yalavarthi S, Shi H, et al. Neutrophil extracellular traps in COVID-19. JCI Insight 2020;5(11).
[19] Schauer C, Janko C, Munoz LE, et al. Aggregated neutrophil extracellular traps limit inflammation by degrading cytokines and chemokines. Nat Med 2014;20(5):511–7.
[20] Jimenez-Alcazar M, Rangaswamy C, Panda R, et al. Host DNases prevent vascular occlusion by neutrophil extracellular traps. Science 2017;358(6367):1202–6.
[21] Leppkes M, Maueroder C, Hirth S, et al. Externalized decondensed neutrophil chromatin occludes pancreatic ducts and drives pancreatitis. Nat Commun 2016;7:10973.
[22] Munoz LE, Boeltz S, Bilyy R, et al. Neutrophil Extracellular Traps Initiate Gallstone Formation. Immunity 2019;51(3):443–50 e4.
[23] Bach-Gansmo ET, Godal HC, Skjonsberg OH. Degradation of fibrinogen and cross-linked fibrin by human neutrophil elastase generates D-like fragments detected by ELISA but not latex D-dimer test. Thromb Res 1998;92(3):125–34.
[24] Belorgey D, Bieth JG. Effect of polynucleotides on the inhibition of neutrophil elastase by mucus proteinase inhibitor and alpha 1-proteinase inhibitor. Biochemistry 1998;37(46):16416–22.
[25] Michels A, Albanez S, Mewburn J, et al. Histones link inflammation and thrombosis through the induction of Weibel-Palade body exocytosis. J Thromb Haemost 2016;14(11):2274–86.
[26] Fuchs TA, Brill A, Duerschmied D, et al. Extracellular DNA traps promote thrombosis. Proc Natl Acad Sci U S A 2010;107(36):15880–5.
[27] Massberg S, Grahl L, von Bruehl ML, et al. Reciprocal coupling of coagulation and innate immunity via neutrophil serine proteases. Nat Med 2010;16(8):887–96.
[28] von Bruhl ML, Stark K, Steinhart A, et al. Monocytes, neutrophils, and platelets cooperate to initiate and propagate venous thrombosis in mice in vivo. J Exp Med 2012;209(4):819–35.
[29] Martinod K, Demers M, Fuchs TA, et al. Neutrophil histone modification by peptidylarginine deiminase 4 is critical for deep vein thrombosis in mice. Proc Natl Acad Sci U S A 2013;110(21):8674–9.
[30] Gosswein S, Lindemann A, Mahajan A, et al. Citrullination Licenses Calpain to Decondense Nuclei in Neutrophil Extracellular Trap Formation. Front Immunol 2019;10:2481.
[31] Abe H, Okajima K, Okabe H, Takatsuki K, Binder BR. Granulocyte proteases and hydrogen peroxide synergistically inactivate thrombomodulin of endothelial cells in vitro. J Lab Clin Med 1994;123(6):874–81.
[32] Zhou P, Yang XL, Wang XG, et al. A pneumonia outbreak associated with a new coronavirus of probable bat origin. Nature 2020;579(7798):270–3.
[33] Hoffmann M, Kleine-Weber H, Schroeder S, et al. SARS-CoV-2 Cell Entry Depends on ACE2 and TMPRSS2 and Is Blocked by a Clinically Proven Protease Inhibitor. Cell 2020;181(2):271–80 e8.
[34] Hamming I, Timens W, Bulthuis ML, Lely AT, Navis G, van Goor H. Tissue distribution of ACE2 protein, the functional receptor for SARS coronavirus. A first step in understanding SARS pathogenesis. J Pathol 2004;203(2):631–7.
[35] Varga Z, Flammer AJ, Steiger P, et al. Endothelial cell infection and endotheliitis in COVID-19. Lancet 2020;395(10234):1417–8.
[36] Ackermann M, Verleden SE, Kuehnel M, et al. Pulmonary Vascular Endothelialitis, Thrombosis, and Angiogenesis in Covid-19. N Engl J Med 2020.
[37] Wichmann D, Sperhake JP, Lutgehetmann M, et al. Autopsy Findings and Venous Thromboembolism in Patients With COVID-19. Ann Intern Med 2020.
[38] Connors JM, Levy JH. COVID-19 and its implications for thrombosis and anticoagulation. Blood 2020;135(23):2033–40.
[39] Beasley MB. The pathologist's approach to acute lung injury. Arch Pathol Lab Med 2010;134(5):719–27.
[40] Bery AI, Hachem RR. Antibody-mediated rejection after lung transplantation. Ann Transl Med 2020;8(6):411.
[41] Jennette JC, Falk RJ, Hu P, Xiao H. Pathogenesis of antineutrophil cytoplasmic autoantibody-associated small-vessel vasculitis. Annu Rev Pathol 2013;8:139–60.
[42] Craddock PR, Hammerschmidt DE, Moldow CF, Yamada O, Jacob HS. Granulocyte aggregation as a manifestation of membrane interactions with complement: possible role in leukocyte margination, microvascular occlusion, and endothelial damage. Semin Hematol 1979;16(2):140–7.

[43] Zwahlen RD, Roth DR, Wyder-Walther M. In vitro aggregation of bovine neonatal neutrophils. A comparative study with adult cattle. Inflammation 1990;14(4):375–87.
[44] Lewis HD, Liddle J, Coote JE, et al. Inhibition of PAD4 activity is sufficient to disrupt mouse and human NET formation. Nat Chem Biol 2015;11(3):189–91.
[45] Giacobbe DR, Battaglini D, Ball L, et al. Bloodstream infections in critically ill patients with COVID-19. Eur J Clin Invest 2020:e13319.
[46] Napirei M, Ludwig S, Mezrhab J, Klockl T, Mannherz HG. Murine serum nucleases–contrasting effects of plasmin and heparin on the activities of DNase1 and DNase1-like 3 (DNase1l3). FEBS J 2009;276(4):1059–73.
[47] Manfredi AA, Rovere-Querini P, D'Angelo A, Maugeri N. Low molecular weight heparins prevent the induction of autophagy of activated neutrophils and the formation of neutrophil extracellular traps. Pharmacol Res 2017;123:146–56.
[48] Wildhagen KC, Garcia de Frutos P, Reutelingsperger CP, et al. Nonanticoagulant heparin prevents histone-mediated cytotoxicity in vitro and improves survival in sepsis. Blood 2014;123(7):1098–101.
[49] Longstaff C, Hogwood J, Gray E, et al. Neutralisation of the anti-coagulant effects of heparin by histones in blood plasma and purified systems. Thromb Haemost 2016;115(3):591–9.
[50] McGonagle D, O'Donnell JS, Sharif K, Emery P, Bridgewood C. Immune mechanisms of pulmonary intravascular coagulopathy in COVID-19 pneumonia. Lancet Rheumatol 2020.